Research article

Modeling of single-lap joints with auxetic adhesive utilizing homogeneous and heterogeneous bondline microstructures

Chatarina P. Puspaningtyas [a], Annisa Jusuf [a],[*], Bambang K. Hadi [a], Arief Yudhanto [b]

[a] Mechanics of Solids and Lightweight Structures Research Group, Faculty of Mechanical and Aerospace Engineering, Institut Teknologi Bandung, Jalan Ganesha 10, Bandung 40132, Indonesia
[b] Department of Mechanical Engineering, Baylor University, Waco, TX 76798, USA

ABSTRACT

Producing lightweight structures can be effectively achieved using adhesive bonding that incorporates a high-performance adhesive, eliminating the mechanical joints (rivet, bolts). Here, the proof-of-concept of tailoring the high-performance adhesive using microstructures exhibiting a negative Poisson's ratio (auxetic) is investigated using two single lap joint (SLJ) models developed in ABAQUS/Standard. The SLJ models consist of two rigid adherends that are bonded using either *homogeneous* or *heterogeneous* adhesive that produces auxetic response. In homogeneous adhesive, a negative value of Poisson's ratio is defined in the adhesive part of the models. In heterogeneous adhesive, the negative Poisson's ratio is obtained by explicitly building orthogonally-arranged elliptical voids in the adhesive part of the models. In addition, the adherend-adhesive interface is represented by cohesive elements with bi-linear traction-separation rule. The effects of using two different adhesive models and thickness on peel and shear stresses, as well as failure mechanism and joint strength, are evaluated. We found that the effect of auxetic adhesive on SLJ response is more profound in the model using heterogeneous adhesive rather than the homogeneous one, where the joint strength enhancement could achieve 45 % in reference to the baseline model. The heterogeneous adhesive embedded between adherends is able to activate ligaments, the mechanism that could not be obtained using merely homogeneous adhesive. Our proposed modeling strategy can be a starting point to further the modeling approach of bonded joints utilizing auxetic adhesive.

1. Introduction

The lightweighting concept in the manufacture of aerospace and automotive structures, either using metallic- or composite-based materials, is often enabled by the adhesive bonding technology, incorporating high-performance adhesive, in replacement of mechanical joining technology using rivets and bolts [1]. Adding to the weight-saving advantage, the adhesive bonding technology also provides a relatively uniform stress distribution between parts, lower fabrication cost, and easier joint preparation than the mechanical fasteners [2]. However, bonding process typically demands a proper preparation of the substrate or adherend surfaces, an extended time for curing of adhesive bondline, the search for a high-performance adhesive, among others [3]. The bonding process may also introduce bondline discontinuity that could affect the safety limit of bonded joint [4]. Moreover, failure of adhesively bonded joints is

typically catastrophic (non-progressive), sending a very minimum warning that clearly jeopardizes the integrity of bonded structures [5]. Thus, an innovative concept to delay the failure process in the adhesive joints is desirable to improve the structural safety.

A number of strategies that have been proposed to enhance the mechanical performance of adhesively bonded joints generally falls within two main categories: substrate modification [6–11] and adhesive modification [12–16]. Substrate modification includes geometrical or surface changes of the substrate, e.g., increasing substrate thickness at the overlapping region, creating a wedge at the substrate tip, making a streamlined thickness transition in the region away from the overlapping region to minimize the load path eccentricity, surface patterning. However, the substrate modification requires additional tooling/machining that incurs extra manufacturing costs [17]. Adhesive modification includes spatial tailoring of the bondline with tough/compliant materials [14], inserting the beaks at the edges of overlapping region [18], applying thermoplastic carrier within adhesive bondline [19]. Nonetheless, the adhesive modification always incorporates foreign features other than the adhesive. A new concept for modifying the adhesive that can be based on the mechanistic approach is still desirable.

In this paper, we explored the application of metamaterial or auxetic concept for the modification of adhesive bondline. Auxetic material is a solid that possesses a negative Poisson's ratio when it is being deformed. It is noteworthy that general isotropic materials may exhibit the 'allowable' Poisson's ratio of $-1 < \nu < 0.5$ [20,21]. Unlike conventional expectations, auxetic material or structure laterally expands upon tensile load and laterally contracts upon compressive load. The auxetic concept/material/structure has been studied at different scales for more than two decades [22,23]. The auxetic materials have been used to create composites and constructions with enhanced shear modulus or indentation resistance [24–26]. Tailoring relative stiffness of a structure based on the beam-crystal structure was used to achieve a specific Poisson's ratio, shear or tensile moduli [27]. Achieving negative Poisson's ratio can be achieved by creating multiple cells with elliptical voids [28] or rotating squares [29,30], which are essentially analogous in terms of mechanism [31]. To the best of authors' knowledge, the exploration of metamaterial or auxetic concept for the adhesive bondline was performed by Athanasiadis et al. [32], showing that their conceptual microstructures could improve the stress transfer between substrates and enhance the joint strength. The conceptual microstructures employing auxetic behavior have, nevertheless, been implemented for improving mechanical performance of sandwich structures and auxetic particle-toughened composites [33–35]. However, further studies on the auxetic concept for adhesive bonded joints are very limited, partly due to the difficulty in the manufacture of auxetic adhesive. Indeed, ordinary adhesive (epoxy, acrylic, urethane, or cyanoacrylate) exhibits a positive Poisson's ratio. The benefit of using adhesive with a negative Poisson's ratio is not yet obvious, but the option for developing a novel adhesive with negative Poisson's ratio needs to be initiated by performing a preliminary computational investigation.

Here, we investigated two modeling routes that may provide better understanding on the effect of auxetic microstructure on adhesively bonded joints. We employed a single lap joint (SLJ) model in the finite element framework using ABAQUS/Standard. Two modeling routes were proposed: (i) SLJ model with *homogeneous* adhesive where positive or negative Poisson's ratio was prescribed as a constant in the model, (ii) SLJ model with *heterogeneous* adhesive where the negative Poisson's ratio was achieved by explicitly building orthogonally-arranged elliptical voids. The orthogonally-arranged elliptical voids were selected due to their simple configuration and minimum stress concentration at the tip of the cut-out. In each model, we investigated the effect of Poisson's ratio on the distribution of stresses (peel and shear), joint strength, and failure mechanisms. We also studied the geometrical effect in the adhesive bondline where adhesive thicknesses were varied (0.2 mm, 2.2 mm, or 3.6 mm). Based on the proposed modeling routes, the advantages and limitations of the SLJ models with either homogeneous or heterogeneous adhesive bondlines are also discussed.

This paper is organized as follows. Section 2 describes the finite element framework where two adhesive models and their modeling procedure are given. Section 3 contains numerical results and discussion pertaining to the experimental validation of SLJ model with thin, homogeneous adhesive, and the effects of auxetic adhesives on stresses, strength, and failure mechanisms. Section 4 concludes our modeling studies with some remarks on further development of the models.
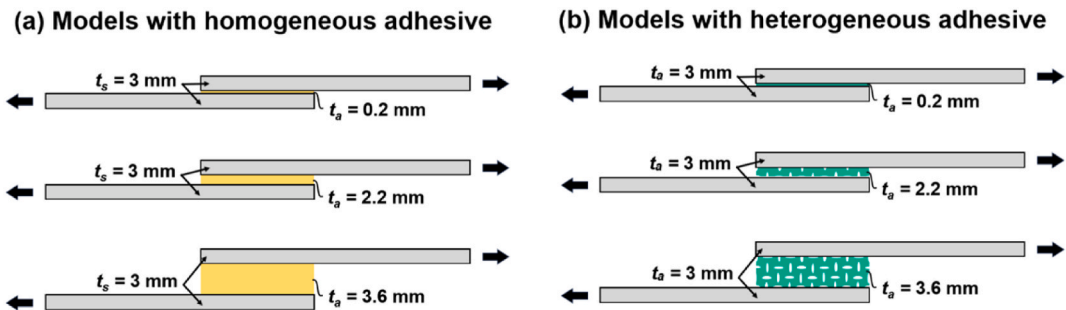
Fig. 1. Single lap joint models with (a) homogeneous adhesive, (b) heterogeneous adhesive. Three different adhesive thicknesses are shown here: 0.2 mm, 2.2 mm, 3.6 mm. Note that the Poisson's ratio in homogeneous adhesive can be positive or negative, while that in heterogeneous adhesive can only be negative due to the auxetic microstructure.

2. Finite element framework

2.1. Description of homogeneous and heterogeneous adhesive models

A single lap joint (SLJ) configuration consisting of two rigid adherends and one adhesive layer was selected to represent the basic bonded joint configuration. The SLJ configuration was also selected to aid the analysis of peel and shear stresses in the adhesive bondline, and the estimation of joint strength. Fig. 1 (a-b) show the SLJ models with homogeneous and heterogeneous, respectively, where three adhesive thicknesses of 0.2, 2.2, and 3.6 mm are also prescribed. The adherend length and thickness were 120 mm and 3 mm, respectively. The overlap length was 25 mm. The negative Poisson's ratio in models with homogeneous adhesive was achieved by merely prescribing a negative value of Poisson's ratio in the isotropic adhesive. On the other hand, the negative Poisson's ratio in models with heterogeneous adhesive was achieved by explicitly building an array of orthogonally-arranged elliptical microvoids that eventually creates a negativity of Poisson's ratio due to tensioning or compression.

Fig. 2 shows a schematic of unit cell with orthogonally-arranged elliptical microvoids. This unit cell was repeatedly arranged across the length and thickness to form multicell of microvoids. It is noteworthy that the original material in heterogeneous adhesive was defined to have a positive value of Poisson's ratio. As mentioned, the orthogonally-arranged elliptical voids could produce a negative Poisson's ratio by modifying geometrical parameters (a, b, L_{min}, L_0) in the unit cells. In this work, we specified Poisson's ratio of -0.5 by prescribing aspect ratio (a/b) and ligament length ratio (L_{min}/L_0) as 20 and 0.2, respectively. In present model, following geometrical values were used: $a = 0.11$ mm, $b = 0.0056$ mm, $L_{min} = 0.04$ mm, $L_0 = 0.2$ mm.

2.2. Finite element modeling

Two-dimensional models of SLJ that consisted of two adherend layers, one adhesive layer, and two cohesive layers (each layer being inserted between adherend and adhesive) were developed in *ABAQUS/Standard* using 4-noded plane-strain elements (CPE4). Fine sized elements of 0.1 mm × 0.1 mm were prescribed for making the finite element mesh of homogeneous models. In heterogeneous models, the local seed of 0.025 mm was prescribed to produce fine sized element mesh. The fine mesh enabled a more accurate analysis of stress distribution at the adhesive midplane. The boundary conditions of the SLJ model were prescribed to resemble the gripping condition of the specimen during the actual test. Left-hand nodes of the lower substrate were constrained in all degrees of freedom. The right-hand nodes of the upper substrate were constrained in *y*-direction, and loaded in *x*-direction with a constant displacement of 0.5 mm.

The adherends were made of aluminum alloy (Al 6082-T651 or Al–Si–Mg–Mn) with a constant thickness of 3 mm. The behavior of the adherends was linear elastic. The mechanical properties of Al 6082-T651 were defined as follows: Young's modulus of 70 GPa, yield strength of 262 MPa, ultimate strength of 324 MPa, failure strain of 21.7 %, and Poisson's ratio of 0.30. The adhesive was epoxy (XN1244) that behaved in elasto-plastic manner. The adhesive has Young's modulus of 5.87 GPa, yield strength of 46.9 MPa, ultimate strength of 68.2 MPa, failure strain of 1.46 %, shear modulus of 2.15 GPa, shear failure strength of 31.6 MPa, shear failure strain of 8.05 %, and Poisson's ratio of 0.35. These mechanical properties were obtained from the experimental data reported by Banea et al. [36].

The interface between adherend and adhesive was modeled using cohesive elements. These cohesive elements were made to obey a bi-linear traction-separation (τ - δ) rule in both normal (n) and shear (s). The constitutive relationship between current traction (τ_n, τ_s) and separation in tension and shear across the cohesive element is seen in Eq. (1).

$$\tau = \begin{Bmatrix} \tau_n \\ \tau_s \end{Bmatrix} = \begin{bmatrix} K_{nn} & K_{ns} \\ K_{ns} & K_{ss} \end{bmatrix} \begin{Bmatrix} \delta_n \\ \delta_s \end{Bmatrix} = [K]\{\delta\} \tag{1}$$
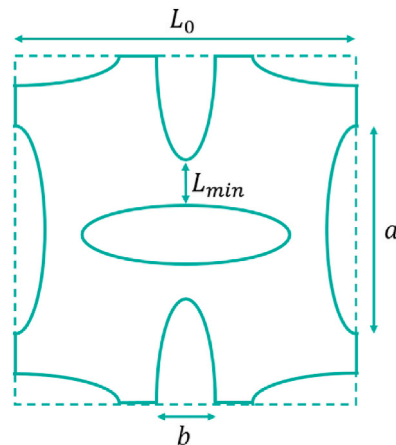
Fig. 2. Unit cell geometric configuration of heterogeneous adhesive.

where $[K]$ represents the slope of first linear region in the traction-separation curve. The traction-separation curve linearly increases up to a point where a criterion is met, thus triggering damage initiation. Eq. (2) shows the damage in the cohesive element initiated when the nominal "quadratic stress criterion" as one of the built-in cohesive failure criteria in the ABAQUS/Standard is equal to 1.0.

$$\left[\frac{\langle\tau_n\rangle}{\tau_n^0}\right]^2 + \left[\frac{\tau_s}{\tau_s^0}\right]^2 = 1 \tag{2}$$

where τ_n^0 is threshold of the tension or compressive tractions, τ_s^0 is threshold of the shear traction. Note that the Macaulay brackets $<>$ indicate that a purely compressive state in the element does not initiate any damage. At this point, the elements started to degrade (physically, the crack or damage started). Thereafter, the propagation regime was represented by the linear degradation of the traction-separation curve. Here, the gradual reduction of the stiffness employed a linear power law that shows a linear softening until material is completely failed as seen in Eq. (3).

$$\frac{G_n}{G_n^c} + \frac{G_s}{G_s^c} = 1 \tag{3}$$

where the area under the traction-separation curve in tension and shear are denoted as G_n and G_s, respectively. G_n^c and G_s^c are critical fracture energy in mode I and mode II (or mode III), respectively, that can be obtained by performing standard fracture tests (double cantilever beam for Mode I, end-notch flexure for Mode II). In our modeling scheme, G_n^c and G_s^c were 0.47 N/mm and 2.20 N/mm, respectively. The normal cohesive stress τ_n^0 and shear cohesive stress τ_s^0 were set as 68 MPa and 32 MPa, respectively. These cohesive parameters are obtained from published references [37–39].

3. Results and discussion

3.1. Experimental validation of SLJ model with positive Poisson's ratio

We validated our SLJ model with homogeneous adhesive of 0.2 mm thickness and adherend thickness of 3 mm using experiments performed by Banea et al. [36]. The adherend surface was treated using grit blasting and acetone degreasing, the adhesive was epoxy with nominal thickness of 0.2 mm. The curing of adhesive joint was performed at 140 °C for 1 h. The lap joint experiments were carried out using universal testing machine under a constant speed of 1 mm/min until the specimen failed. The comparison between our model and experimental data is displayed in Fig. 3. It is shown that the force-displacement curve of SLJ model was in a good agreement with that of experiment. Our SLJ model with two rigid adherends, one adhesive layers (0.2 mm) and two cohesive layers was able to emulate the experimental test result with a good accuracy, suggesting that the model was trustworthy to further investigate the mechanical response of SLJ with different adhesive thickness or auxetic adhesive layer.

3.2. Effect of auxetic adhesive on distribution of stresses

3.2.1. Distribution of stresses based on the analytical model of Goland-Reissner

The effect of using auxetic adhesive as a bondline of SLJ configuration is analytically studied using a well-known Goland-Reissner approach [40], where the distribution of peel and shear stresses are evaluated. The detailed theoretical treatment of Goland-Reissner approach can be reviewed in the Appendix. Fig. 4a shows that the distribution of peel stress was constant along the bondline regardless
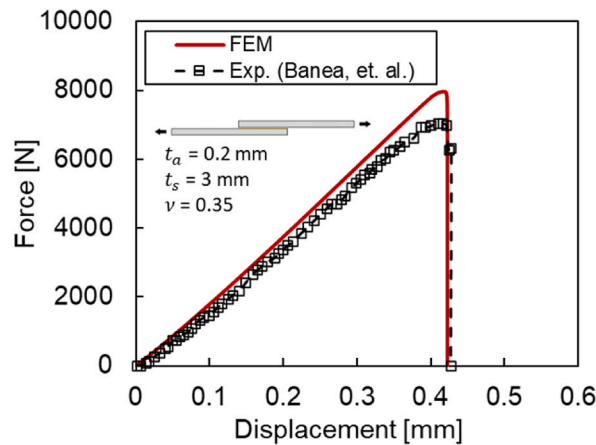
Fig. 3. Comparison of force-displacement responses in SLJ with 0.2 mm adhesive thickness between finite element method (FEM) and experiment [36].
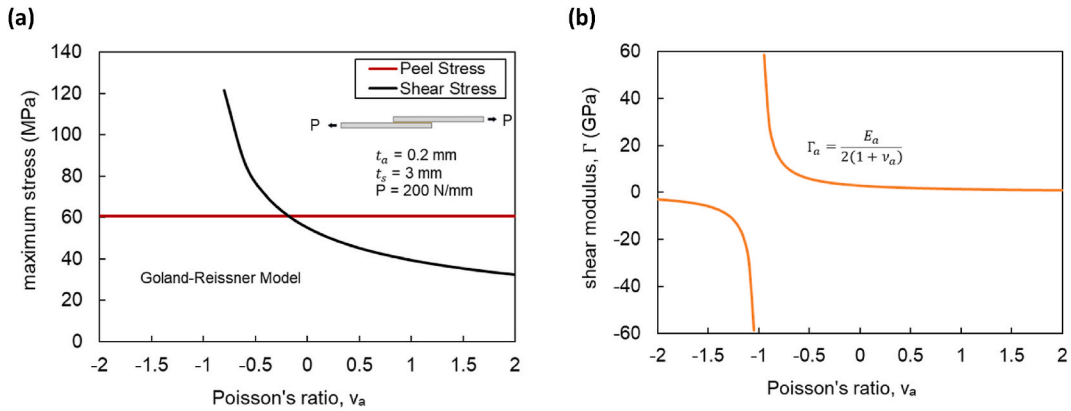
Fig. 4. The relationship between Poisson's ratio v with (a) maximum stress in the bondline and (b) shear modulus Γ_a. The shear stress and shear modulus become asymptotic as the Poisson's ratio reaches the value of -1.

of whether the Poisson's ratio is positive or negative. In contrast, shear stress along the bondline was affected by the Poisson's ratio. The shear stress was asymptotic towards a higher magnitude as the Poisson's ratio approached -1. The reason for this asymptotic behavior was the fact that the shear stress calculation incorporates coefficient β that affected Poisson's ratio ν_a and corresponding shear modulus Γ_a (for isotropic materials). Fig. 4b shows the relationship between shear modulus and Poisson's ratio for isotropic material employed in our model, showing the asymptotic behavior as the Poisson's ratio approached -1. To conclude, as the Goland-Reissner analytical approach could only capture the effect of Poisson's ratio on the shear stress distribution only, we thus
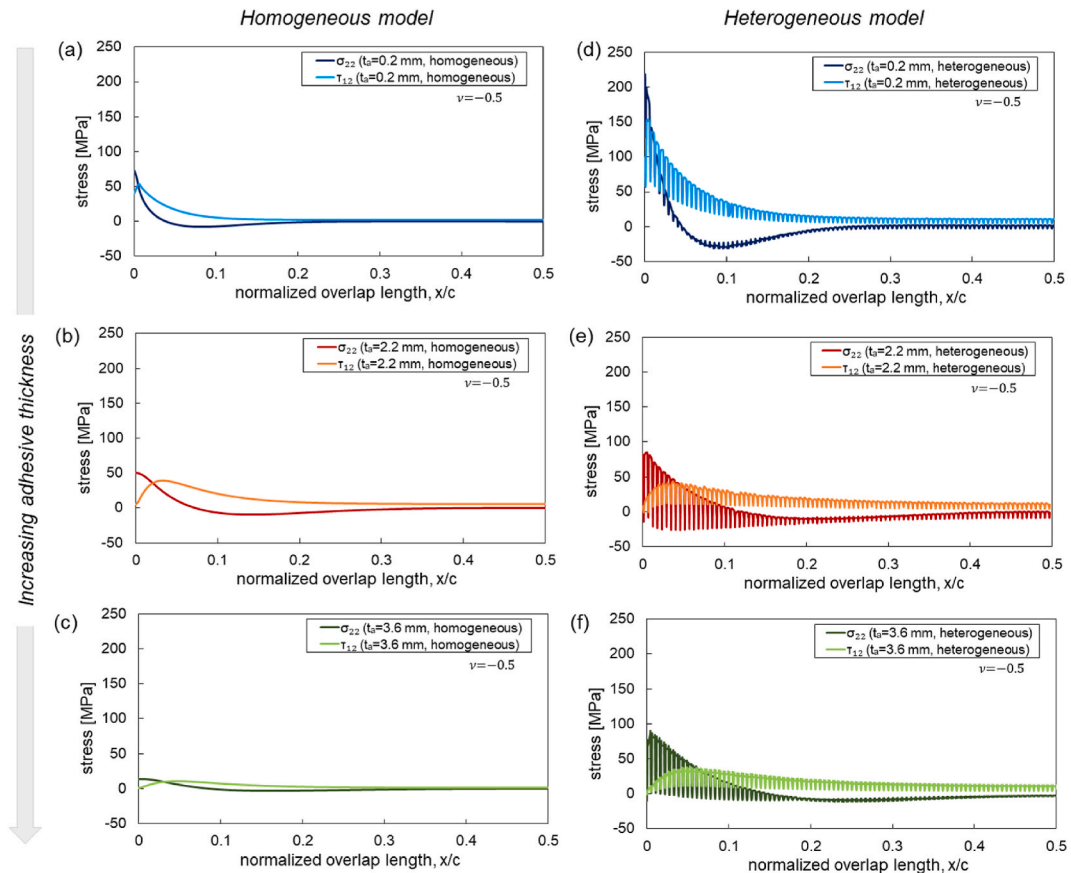
Fig. 5. Distribution of peel stress (σ_{22}) and shear stress (τ_{12}) in the mid-plane of adhesive bondline using adhesive of different thickness: (a) homogeneous, $t_a = 0.2$ mm, (b) homogeneous, $t_a = 2.2$ mm, (c) homogeneous, $t_a = 3.6$ mm, (d) heterogeneous, $t_a = 0.2$ mm, (e) heterogeneous, $t_a = 2.2$ mm, (f) heterogeneous, $t_a = 3.6$ mm.

resorted to the FEM that provided a more reliable outcome of both peel and shear stress distribution. The following section provides the distribution of stresses obtained by FEM.

3.2.2. Distribution of stresses based on the finite element models

The effect of Poisson's ratio on the distribution of peel stress (σ_{22}) and shear stress (τ_{12}) in SLJ with homogeneous and heterogeneous adhesives of different thickness are given in Fig. 5a–c and Fig. 5d–f, respectively. In SLJ model with either homogeneous or heterogeneous adhesive, thinner adhesive introduces higher stress amplification than the thinner one as the stress transfer from adherend to the adhesive was more profound in thinner adhesive than the thicker one. In other words, producing thicker adhesive seems to be a feasible solution for reducing stresses, that may delay the final failure. Although thicker adhesive may not be a preferable solution from a structural standpoint as the geometry becomes thicker, while the weight and cost may also increase, thick bondline may be applicable for structures incorporating thick interfaces such as wind turbine blades, where its thickness can go up into a few centimeters [41,42]. In addition, the location of stress amplification is not affected by the adhesive model selected in the SLJ configuration. In SLJ with homogeneous adhesive, increasing adhesive thickness t_a while keeping adherend thickness t_s constant at 3 mm results in the decrease of maximum peel and shear stresses at the edges. Likewise, SLJ models with heterogeneous adhesive experienced an increase of maximum peel and shear stresses at the edges.

However, as shown in Fig. 5d–f, heterogeneous adhesive introduced a fluctuation of both peel and shear stresses across the bondline. We then compared closely the peel stress distribution in SLJ with homogeneous and heterogeneous adhesives by selecting 2.2 mm thick adhesive. Fig. 6 shows the stress distribution in the mid-plane of adhesive bondline of SLJ with homogeneous and heterogeneous adhesives. While the homogeneous adhesive produced constant stresses across the overlapping region (Fig. 6a), the horizontal elliptical voids produced higher stresses as compared to other features (vertical elliptical voids, or pure adhesive region between voids). The horizontal elliptical voids are more sensitive to the normal and shear loading introduced into the SLJ configuration than the vertical ones. The peak of peel stress fluctuation can reach 3–4 times higher than that of shear stress fluctuation, showing that the stress state acting on the adhesive is dominated by the peeling action rather than the shearing action.

3.3. Effect of auxetic adhesive on strength and failure mechanism

The quasi-static simulation was performed on the SLJ models with homogeneous and heterogeneous adhesive in ABAQUS/Standard up to failure. The load-displacement curves obtained from the FEM simulation are shown in Fig. 7. In SLJ models with 0.2 mm adhesive thickness (left), homogeneous and heterogeneous adhesive did not produce a significant difference in terms failure onset (failure load or displacement onset). The elastic energy being dissipated during the loading increment in homogeneous and heterogeneous adhesive was similar. Here, it is evident that negative Poisson's ratio is insensitive to the type of adhesive modeling, either homogeneous or heterogeneous, implemented in SLJ configuration. As the adhesive thickness in SLJ model was increased to 2.2 mm or 3.6 mm, initial slope of load-displacement curves and maximum failure load of SLJ model were reduced. SLJ becomes less stiff as the
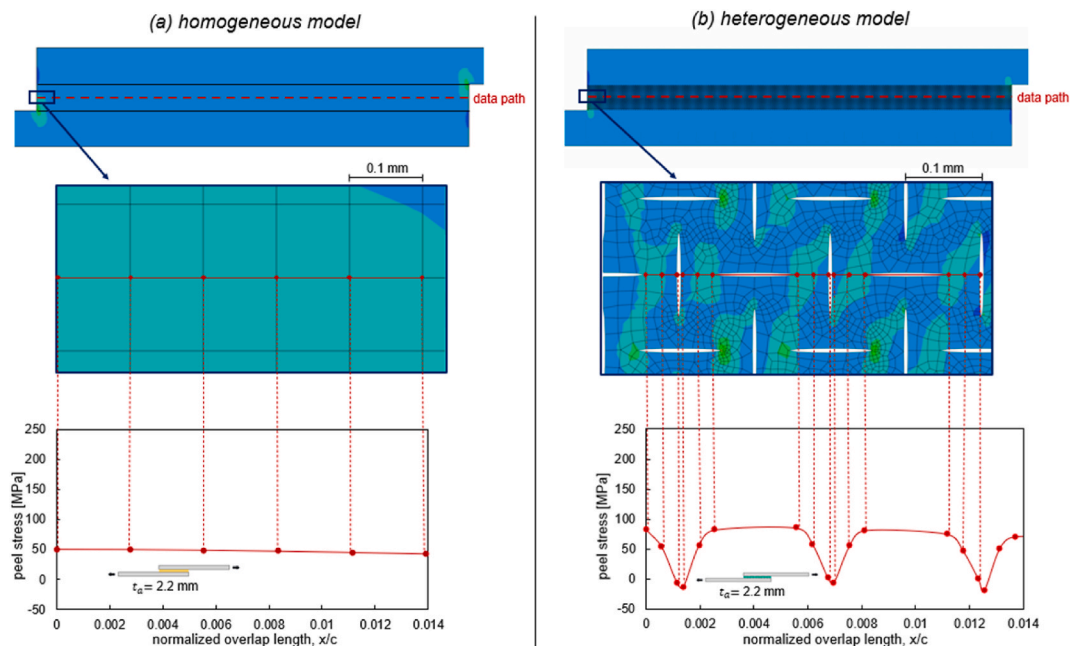
Fig. 6. Comparison of peel stress distribution at the edge of mid-plane adhesive bondline for SLJ models with t_a = 2.2 mm: (a) homogeneous adhesive model, (b) heterogeneous adhesive model.
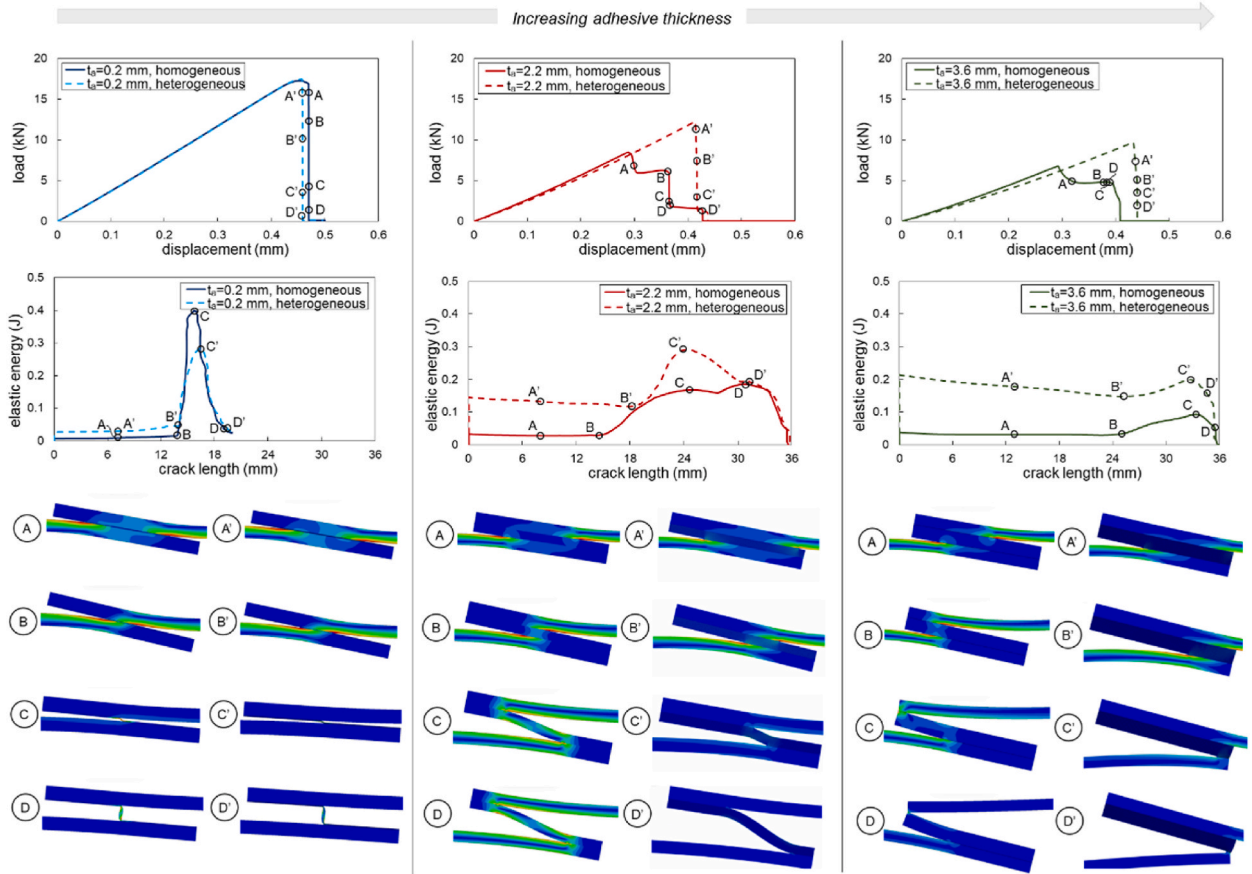
Fig. 7. Load-displacement curves and elastic energy absorbed by the adhesive for different thickness: $t_a = 0.2$ mm (left), $t_a = 2.2$ mm (middle), and $t_a = 3.6$ mm (right) for both homogeneous (A, B, C, D) and heterogeneous (A′, B′, C′, D′).

adhesive took over some of the loads. Thicker adhesive also introduced the eccentricity of the load path, producing high bending moment to compensate such a joint eccentricity. It is important to note that SLJ models with heterogeneous adhesive resulted in a higher joint strength of up to 45 % in comparison to that of homogeneous adhesive.

The effectiveness of heterogeneous adhesive to capture a higher failure load than homogeneous adhesive was investigated by plotting the crack length – elastic energy dissipation during the stage-by-stage deformation (Point A-D) that are shown in Fig. 7. In general, Fig. 7 shows that both homogeneous and heterogeneous adhesives with thin adhesive (0.2 mm) reached similar peak of energy dissipation at around the middle of overlapping area (16–17 mm). The homogeneous model could absorb up to 0.4 J at Point C, whereas heterogeneous model could absorb up to 0.3 J at Point C'. This peak of energy dissipation was strongly correlated with the stretching of macroscopic ligament between adherends, minimizing the influence of possible stretching (due to negative Poisson's ratio) of adhesive region between elliptical voids in the heterogeneous model. As the adhesive thickness was increased to 2.2 mm or 3.6 mm, the energy dissipation in heterogeneous adhesive (0.14 J or 0.21 J, respectively; see Point A and A′) was higher than that in homogeneous adhesive since the beginning of the crack. The additional energy was provided by the deformation of microscopic ligaments between elliptical voids. Point B and B′ in homogeneous and heterogeneous adhesive, respectively, indicates the increase of total energy dissipation due to macroscopic ligament between adherends, which was higher in the heterogeneous adhesive than the homogeneous one. The peak of energy was located at Point C or C′ in Fig. 7 that is associated with the further propagation of crack at the interface. Here, the negative Poisson's ratio in heterogeneous model produced a contraction at the edges of bondline, and compression at the inner bondline. As a result, total energy dissipation due to both microscopic ligaments between microvoids and macroscopic ligaments between adherends produced higher failure load than that in homogeneous adhesive. Note that as the adhesive becomes thicker (3.6 mm) the benefit of heterogeneous model for representing negative Poisson's ratio becomes apparent. The crack in heterogeneous adhesive grew only on one interface, while that in homogeneous adhesive grew on two interfaces. Higher energy dissipation in 3.6 mm thick adhesive was being dissipated mostly through by the accumulation of microscopic ligaments due to microvoids, in addition to cohesive failure.

3.4. Remarks on homogeneous and heterogeneous adhesive models

Several remarks associated with advantage and limitation of using either homogeneous or heterogeneous adhesive in SLJ models is briefly discussed here. The advantage of using homogeneous adhesive is the ease of implementation as one can readily build a homogeneous part by merely defining a negative Poisson's ratio rather than prescribing a microstructure that produces negative Poisson's ratio. However, SLJ model with homogeneous adhesive is limited by its inability to activate additional energy dissipation mechanism due to a complex deformation of auxetic microstructures, e.g., ligament formation. On the other hand, SLJ model with heterogeneous adhesive is thus more realistic in which the ligament formation contributing to the total energy dissipation during decohesion process can be simulated. However, the heterogeneous adhesive is much more complex in terms of finite element model development where multiple unit cells having, for instance, re-entrant microstructures should be precisely modeled. In both models, experimental validation is yet to be performed due to the fact that existing technologies (existence of adhesive with auxetic behavior or relatively low resolution of 3D printing for producing thin adhesive with auxetic microstructures) have not been available for supporting the validation. Nonetheless, this work provides a modeling framework towards a path of novel adhesive configuration for bonded joints.

4. Conclusions

The effect of using adhesive layer with negative Poisson's ratio was investigated by developing single-lap joint models with homogeneous and heterogeneous adhesives. Effect of adhesive thickness was also studied in terms of stress distribution, joint strength and failure mechanisms. Cohesive elements were implemented in two interfaces of bonded joint for simulating the failure. We found that the analytical model proposed by Goland and Reissner was able to estimate only the shear stress distribution in adhesive with negative Poisson's ratio, but unable to estimate the peel stress distribution. The finite element models of single-lap joints with either homogeneous or heterogeneous adhesive developed here were able to estimate the effect of negative Poisson's ratio on shear and peel stresses, joint strength and the failure mechanisms. Our modeling frameworks showed that bonded joint with heterogeneous adhesive with auxetic behavior (as represented by the multiple orthogonally-arranged elliptical voids) could improve the joint strength of up to 45 % as compared to the homogeneous auxetic adhesive as the adhesive becomes thicker (2.2 or 3.6 mm). Orthogonally-arranged elliptical microvoids built in single-lap joint with heterogeneous adhesive enabled the formation of microscopic ligaments that provide extra elastic energy dissipation that eventually enhanced the joint strength. Our modeling framework of single-lap joint with heterogeneous adhesive is a promising step towards the future predictive models utilizing adhesive with negative Poisson's ratio generated by a more complex microstructure.

Additional information

No additional information is available for this paper.

CRediT authorship contribution statement

Chatarina P. Puspaningtyas: Writing - original draft, Investigation, Formal analysis, Data curation. **Annisa Jusuf:** Writing - review & editing, Supervision, Funding acquisition, Formal analysis, Conceptualization. **Bambang K. Hadi:** Writing - review & editing, Supervision, Formal analysis, Conceptualization. **Arief Yudhanto:** Writing - review & editing, Supervision, Methodology, Formal analysis, Conceptualization.

Declaration of competing interest

The authors declare that they have no known competing financial interests or personal relationships that could have appeared to influence the work reported in this paper.

Appendix

We employed the theoretical model proposed by Goland and Reissner for evaluating the stress distribution along thin adhesive bondline in the SLJ model with rigid substrate. Upon the application of tensile loading on the single-lap joint, the bending moment M and transversal force V can be calculated, respectively, as in Eq. (4) and Eq. (5)

$$M = k \frac{\overline{P} t_s}{2} \tag{4}$$

$$V = k' \frac{\overline{P} t_s}{2} \tag{5}$$

where $\overline{P}$ is the tensile force per unit width, t_s is the thickness of substrate/adherend, k is the bending moment factor, k' is transversal force factor. k and k' would be 1.0 when the substrate is very rigid (no rotation). In contrast, k and k' would be very small ($\ll 1.0$) if substrate is flexible (rotation). k can be calculated as in Eq. (6)

$$k = \frac{\cosh(u_2 c)}{\cosh(u_2 c) + 2\sqrt{2}\sinh(u_2 c)} \tag{6}$$

in which c is half of the overlap length, u_2 can be calculated as in Eq. (7)

$$u_2 = \sqrt{\frac{3(1 - \nu^2)}{2}} \frac{1}{t_s} \sqrt{\frac{\overline{P}}{t_s E_s}} \tag{7}$$

where ν_s is the Poisson's ratio of substrate, E_s is substrate's Young's modulus. k' can be calculated as in Eq. (8)

$$k' = \frac{kc}{t_s} \sqrt{3(1 - \nu^2) \frac{\overline{P}}{t_s E_s}} \tag{8}$$

The distribution of shear stress along the adhesive bondline can calculated as in Eq. (9)

$$\tau(x) = -\frac{\overline{P}}{8c} \left(\frac{\beta c}{t_s} (1 + 3k) \frac{\cosh\left(\frac{\beta x}{t_s}\right)}{\sinh\left(\frac{\beta c}{t_s}\right)} + 3(1 - k) \right) \tag{9}$$

β can be calculated as in Eq. (10)

$$\beta = \sqrt{\frac{8\Gamma_a t_s}{E_s t_a}} \tag{10}$$

in which Γ_a is the shear modulus of adhesive, t_a is the thickness of adhesive. Assuming an isotropic adhesive, Γ_a can be calculated as in Eq. (11)

$$\Gamma_a = \frac{E_a}{2(1 + \nu_a)} \tag{11}$$

The distribution of peel stress along the adhesive bondline can be calculated as Eq. (12) – Eq. (18)

$$\sigma(x) = \frac{1}{\Delta} \frac{\overline{P} t_s}{c^2} [A + B] \tag{12}$$

where

$$\Delta = \frac{1}{2} (\sin(2\lambda) + \sinh(2\lambda)) \tag{13}$$

$$A = \left(R_2 \lambda^2 \frac{k}{2} + \lambda k' \cosh(\lambda)\cos(\lambda) \right) \cosh\left(\frac{\lambda x}{c}\right) \cos\left(\frac{\lambda x}{c}\right) \tag{14}$$

$$B = \left(R_1 \lambda^2 \frac{k}{2} + \lambda k' \sinh(\lambda)\sin(\lambda) \right) \sinh\left(\frac{\lambda x}{c}\right) \sin\left(\frac{\lambda x}{c}\right) \tag{15}$$

in which

$$\lambda = \frac{c}{t_s} \left(6 \frac{E_a}{E_s} \frac{t_s}{t_a} \right)^{1/4} \tag{16}$$

$$R_1 = \cosh(\lambda)\sin(\lambda) + \sinh(\lambda)\cos(\lambda) \tag{17}$$

$$R_2 = -\cosh(\lambda)\sin(\lambda) + \sinh(\lambda)\cos(\lambda) \tag{18}$$

Here, it is evident that the Poisson's ratio of adhesive would affect only the distribution of shear stress distribution along the bondline rather than that of the peel stress.

References

[1] A. Higgins, Adhesive bonding of aircraft structures, Int. J. Adhesion Adhes. 20 (5) (2000) 367–376, https://doi.org/10.1016/S0143-7496(00)00006-3. Jan.

[2] L.F.M. Da Silva, A. Öchsner, R.D. Adams, "Handbook of Adhesion Technology", second ed., Springer, 2018.

[3] A. Yudhanto, M. Alfano, G. Lubineau, Surface preparation strategies in secondary bonded thermoset-based composite materials: a review, Compos Part A Appl Sci Manuf 147 (2021) 106443, https://doi.org/10.1016/j.compositesa.2021.106443. Aug.

[4] S. Heide-Jørgensen, M.K. Budzik, Effects of bondline discontinuity during growth of interface cracks including stability and kinetic considerations, J Mech Phys Solids 117 (2018) 1–21, https://doi.org/10.1016/j.jmps.2018.04.002. Aug.

[5] X. Zhao, R.D. Adams, L.F.M. da Silva, Single lap joints with Rounded adherend corners: experimental results and strength prediction, J. Adhes. Sci. Technol. 25 (8) (2011) 837–856, https://doi.org/10.1163/016942410X520880. Jan.

[6] A. Wagih, R. Tao, A. Yudhanto, G. Lubineau, Improving mode II fracture toughness of secondary bonded joints using laser patterning of adherends, Compos Part A Appl Sci Manuf 134 (2020) 105892, https://doi.org/10.1016/j.compositesa.2020.105892. Jul.

[7] J. Alyousef, A. Yudhanto, R. Tao, G. Lubineau, Laser ablation of CFRP surfaces for improving the strength of bonded scarf composite joints, Compos. Struct. 296 (2022) 115881, https://doi.org/10.1016/j.compstruct.2022.115881. Sep.

[8] M. Alfano, G. Ambrogio, F. Crea, L. Filice, F. Furgiuele, Influence of laser surface modification on bonding strength of Al/Mg adhesive joints, J. Adhes. Sci. Technol. 25 (11) (2011) 1261–1276, https://doi.org/10.1163/016942410X533381. Jan.

[9] C. Morano, L. Bruno, L. Pagnotta, M. Alfano, Analysis of crack trapping in 3D printed bio-inspired structural interfaces, Procedia Struct. Integr. 12 (2018) 561–566, https://doi.org/10.1016/j.prostr.2018.11.063.

[10] R. Tao, M. Alfano, G. Lubineau, Laser-based surface patterning of composite plates for improved secondary adhesive bonding, Compos Part A Appl Sci Manuf 109 (2018) 84–94, https://doi.org/10.1016/j.compositesa.2018.02.041. Jun.

[11] R. Tao, M. Alfano, G. Lubineau, In situ analysis of interfacial damage in adhesively bonded composite joints subjected to various surface pretreatments, Compos Part A Appl Sci Manuf 116 (2019) 216–223, https://doi.org/10.1016/j.compositesa.2018.10.033. Jan.

[12] L.F.M. da Silva, M.J.C.Q. Lopes, Joint strength optimization by the mixed-adhesive technique, Int J Adhes 29 (5) (2009) 509–514, https://doi.org/10.1016/j.ijadhadh.2008.09.009. Jul.

[13] J.F. Durodola, Functionally graded adhesive joints – a review and prospects, Int J Adhes 76 (2017) 83–89, https://doi.org/10.1016/j.ijadhadh.2017.02.008. Jul.

[14] S. Kumar, B.L. Wardle, M.F. Arif, Strength and performance enhancement of bonded joints by spatial tailoring of adhesive compliance via 3D printing, ACS Appl. Mater. Interfaces 9 (1) (2017) 884–891, https://doi.org/10.1021/acsami.6b13038. Jan.

[15] M. Budzik, J. Jumel, K. Imieli`nska, M.E.R. Shanahan, Effect of adhesive compliance in the assessment of soft adhesives with the wedge test, J. Adhes. Sci. Technol. 25 (1–3) (2011) 131–149, https://doi.org/10.1163/016942410X501133. Jan.

[16] A. Pascuzzo, A. Yudhanto, M. Alfano, G. Lubineau, On the effect of interfacial patterns on energy dissipation in plastically deforming adhesive bonded ductile sheets, Int J Solids Struct 198 (2020) 31–40, https://doi.org/10.1016/j.ijsolstr.2020.04.001. Aug.

[17] R. Abbott, "Analysis and Design of Composite and Metallic Flight Vehicle Structures", second ed., Abbott Aerospace SEZC Ltd, 2018.

[18] J.Y. Cognard, Numerical analysis of edge effects in adhesively-bonded assemblies' application to the determination of the adhesive behaviour, Comput. Struct. 86 (17–18) (2008) 1704–1717, https://doi.org/10.1016/j.compstruc.2008.02.003. Sep.

[19] S. Heide-Jørgensen, S. Teixeira de Freitas, M.K. Budzik, On the fracture behaviour of CFRP bonded joints under mode I loading: effect of supporting carrier and interface contamination, Compos. Sci. Technol. 160 (2018) 97–110, https://doi.org/10.1016/j.compscitech.2018.03.024. May.

[20] K.W. Wojciechowski, "Remarks on 'Poisson ratio beyond the limits of the elasticity theory,'", J Physical Soc Japan 72 (7) (2003) 1819–1820, https://doi.org/10.1143/JPSJ.72.1819. Jul.

[21] R. Lakes, K.W. Wojciechowski, Negative compressibility, negative Poisson's ratio, and stability, Phys. Status Solidi 245 (3) (2008) 545–551, https://doi.org/10.1002/pssb.200777708. Feb.

[22] K.E. Evans, M.A. Nkansah, I.J. Hutchinson, S.C. Rogers, Molecular network design, Nature 353 (6340) (1991), https://doi.org/10.1038/353124a0, 124–124, Sep.

[23] D. Prall, R.S. Lakes, Properties of a chiral honeycomb with a Poisson's ratio of -1, Int. J. Mech. Sci. 39 (3) (1997) 305–314, https://doi.org/10.1016/S0020-7403(96)00025-2. Mar.

[24] J.B. Choi, R.S. Lakes, Non-linear properties of polymer cellular materials with a negative Poisson's ratio, J. Mater. Sci. 27 (17) (1992) 4678–4684, https://doi.org/10.1007/BF01166005.

[25] J.B. Choi, R.S. Lakes, Non-linear properties of metallic cellular materials with a negative Poisson's ratio, J. Mater. Sci. 27 (19) (1992) 5375–5381, https://doi.org/10.1007/BF02403846. Oct.

[26] K.E. Evans, A. Alderson, Auxetic materials: functional materials and structures from lateral thinking, Adv. Mater. 12 (9) (2000) 617–628, https://doi.org/10.1002/(SICI)1521-4095(200005)12:9<617::AID-ADMA617>3.0.CO;2-3. May.

[27] T.P. Hughes, A. Marmier, K.E. Evans, Auxetic frameworks inspired by cubic crystals, Int J Solids Struct 47 (11–12) (2010) 1469–1476, https://doi.org/10.1016/j.ijsolstr.2010.02.002. Jun.

[28] T.-C. Lim, Elasticity of Auxetic Solids, 2015, pp. 107–145, https://doi.org/10.1007/978-981-287-275-3_3.

[29] J.N. Grima, K.E. Evans, Auxetic behavior from rotating squares, J. Mater. Sci. Lett. 19 (17) (2000) 1563–1565, https://doi.org/10.1023/A:1006781224002.

[30] M. Taylor, L. Francesconi, M. Gerendás, A. Shanian, C. Carson, K. Bertoldi, Low porosity metallic periodic structures with negative Poisson's ratio, Adv. Mater. 26 (15) (2014) 2365–2370, https://doi.org/10.1002/adma.201304464. Apr.

[31] T.-C. Lim, Analogies across auxetic models based on deformation mechanism (Phys. Status Solidi RRL 6/2017), Phys. Status Solidi Rapid Res. Lett. 11 (6) (2017) 1770330, https://doi.org/10.1002/pssr.201770330. Jun.

[32] A.E.F. Athanasiadis, M.A. Dias, M.K. Budzik, Can confined mechanical metamaterials replace adhesives? Extreme Mech Lett 48 (2021) 101411 https://doi.org/10.1016/j.eml.2021.101411. Oct.

[33] P.H. Cong, N.D. Duc, Nonlinear dynamic analysis of porous eccentrically stiffened double curved shallow auxetic shells in thermal environments, Thin-Walled Struct. 163 (2021) 107748.

[34] P.H. Cong, P.K. Quyet, N.D. Duc, Effects of lattice stiffeners and blast load on nonlinear dynamic response and vibration of auxetic honeycomb plates, Proc. IME C J. Mech. Eng. Sci. 235 (23) (2021) 7192–7211, https://doi.org/10.1177/0954406221992797.

[35] N.T. Duong, N.D. Duc, Evaluation of elastic properties and thermal expansion coefficient of composites reinforced by randomly distributed spherical particles with negative Poisson's ratios, Compos. Struct. 153 (2016) 569–577.

[36] M.D. Banea, L.F.M. da Silva, R.D.S.G. Campilho, Effect of temperature on the shear strength of aluminum single lap bonded joints for high temperature applications, J. Adhes. Sci. Technol. 28 (14–15) (2014) 1367–1381, https://doi.org/10.1080/01694243.2012.697388. Jul.

[37] M.D. Banea, L.F.M. da Silva, R.D.S.G. Campilho, Effect of temperature on tensile strength and mode I fracture toughness of a high temperature epoxy adhesive, J. Adhes. Sci. Technol. 26 (7) (2012) 939–953, https://doi.org/10.1163/156856111X593649. Apr.

[38] M.D. Banea, L.F.M. da Silva, R.D.S.G. Campilho, Mode I fracture toughness of adhesively bonded joints as a function of temperature: experimental and numerical study, Int J Adhes 31 (5) (2011) 273–279, https://doi.org/10.1016/j.ijadhadh.2010.09.005. Jul.

[39] M.D. Banea, L.F.M. da Silva, R.D.S.G. Campilho, Mode II fracture toughness of adhesively bonded joints as a function of temperature: experimental and numerical study, J. Adhes. 88 (4–6) (2012) 534–551, https://doi.org/10.1080/00218464.2012.660835. Apr.

[40] R.D.S.G. Campilho, "Strength Prediction of Adhesively-Bonded Joints", Taylor & Francis, CRC Press, 2017 https://doi.org/10.1201/9781315370835.

[41] D. Zarouchas, R. Nijssen, Mechanical behaviour of thick structural adhesives in wind turbine blades under multi-axial loading, J. Adhes. Sci. Technol. 30 (13) (2016) 1413–1429, https://doi.org/10.1080/01694243.2016.1146392. Jul.

[42] L. Mishnaevsky, K. Branner, H. Petersen, J. Beauson, M. McGugan, B. Sørensen, Materials for wind turbine blades: an overview, Materials 10 (11) (2017) 1285, https://doi.org/10.3390/ma10111285. Nov.